

Synthesis and shaping scale-up study of functionalized UiO-66 MOF for ammonia air purification filters

Yoldes Khabzina⁽¹⁾, Jeremy Dhainaut⁽¹⁾, Mehdi Bessaa⁽¹⁾, Matthias Ahlhelm⁽²⁾, Hans-Juergen Richter⁽²⁾, Helge Reinsch^(3,4), Norbert Stock⁽³⁾, David Farrusseng^{(1)*}

⁽¹⁾Université de Lyon 1, UMR CNRS 5256, Institut de recherches sur la catalyse et l'environnement, IRCELYON, 2 Ave Albert Einstein, F-69626 Villeurbanne, France.

⁽²⁾Fraunhofer-Institute for Ceramic Technologies and Systems (IKTS), Winterbergstrasse 28, 01277 Dresden, Germany.

⁽³⁾Institut für Anorganische Chemie, CAU Kiel, Max-Eyth-Straße 2, 24118 Kiel, Germany.

⁽⁴⁾MOF Application Services, 25-27 rue Tronchet, 75008 Paris, France

KEYWORDS. Ammonia adsorption, breakthrough measurements, UiO66-COOH

ABSTRACT: We report herein the upscaled synthesis and shaping of UiO66-COOH for NH₃ air purification. The synthesis of the zirconium-based MOF was carried out in a batch reactor in an aqueous suspension with a yield of 89% and a space-time yield of 350 kg/day/m³. Neither toxic chemicals nor organic solvents were used, allowing this MOF to be employed in individual or collective air purification devices. Freeze-granulation and extrusion shaping techniques were investigated. The NH₃ air purification performances of UiO66-COOH in bead, tablet and extrudate forms were compared to those of commercial carbon based materials (3M and Norit). Testing conditions were chosen to reflect current standards for ammonia concentration (600-1200 ppm) and velocity. In addition, the breakthrough measurements were carried out at three different relative humidity levels (0%, 40% and 70%). Pellets and extrudates of UiO66-COOH outperformed commercial benchmark adsorbents in all conditions, especially in dry conditions, for which the commercial adsorbents suffered impaired ammonia uptake and shortened service life. Extrudates of UiO66-COOH also withstood attrition after intensive shaking.

INTRODUCTION

Impregnated carbons are state-of-the-art adsorbents for ammonia air purification. They are commercialized in the form of type K cartridges for individual gas protection. They show poor aging characteristics, however, due to deleterious interactions of the mobile active phase with the carbon¹. Various studies have investigated how MOFs perform for the air filtering of Toxic Industrial Chemicals (TIC), particularly NH₃^{1,2,3,4,5,6,7,8,9,10,11}. For the latter, high ammonia adsorption capacities under both dry and humid conditions have been dynamically measured for UiO-66-NH₂, Ni-CPO-27, Fe-MIL-100 and HKUST-1¹². It was underlined that in addition to adsorption performances, the chemical and mechanical stabilities and cost issues should also be addressed¹². Extra factors to carefully consider are process and user safety. Unfortunately, up to now, MOFs have usually been synthesized in organic solvents such as DMF, especially those being tested for TIC abatement^{2,3,13,14,15,1,6,7,9}. DMF is a toxic chemical considered to present a health hazard: it can cause various accidents and birth defects¹⁶, its inhalation results in liver damage, and it causes digestive disturbances in workers¹⁷. As a consequence, DMF should not be used as the synthesis solvent for breathable air filtration devices even if extensive washing is carried out.

Shaping the adsorbent with the appropriate particle size and density is a practical prerequisite. In an individual protection cartridge, the size of the adsorbent grains is generally between 12 and 20 mesh¹⁸ (corresponding to 1680

- 840 µm). Smaller particles would result in an excessive pressure drop, i.e., breathing resistance, which cannot be accepted by the users⁵. For the same reason, the shaped adsorbent must not decompose into fine particles upon shaking or similar mechanical stress. Although it is acknowledged that shaping processes can often affect performances in comparison to the original powder, the effect of shaping on adsorption capacities is rarely reported^{1,12}, especially regarding the volumetric adsorption capacity. Indeed, to the best of our knowledge, adsorption capacity is always reported by unit of mass, yet volumetric capacity is a key criterion because the cartridge volume is limited, especially for face mask filters. Unfortunately, both bulk and tapped densities of shaped MOFs are rarely reported, thereby preventing the volumetric extrapolation of uptakes^{19,20}. In addition, novel adsorbents are rarely benchmarked under relevant conditions, rendering impossible any rational comparison with suitable commercial adsorbents for the application in question. This is the case not only for service lifetime, i.e., breakthrough time, but also for aging and mechanical stability.

Among MOF candidates that have shown high NH₃ adsorption capacities in dynamic and humid conditions, UiO-type MOFs are recognized to be exceptionally stable over a wide range of pH, humidity, temperature and pressure conditions^{5,21,22}. The UiO-66 class is based on Zr₆O₄(OH)₄ octahedral nodes that form lattices in an ideal 12-fold coordination with dicarboxylic linkers, resulting in

a cubic close-packed unit cell structure. The high zirconium charge and the elevated connectivity of the nodes account for exceptionally good chemical, thermal and mechanical resistance^{5,23}. Following the suggestions of Kim et al.⁸, it was anticipated that functionalizing the UiO-66 with free carboxylic acid would facilitate NH₃ adsorption by Brønsted-type acid-base interactions. Recently, Joshi et al. showed that solid UiO66-COOH made from 1,2,4-benzenetricarboxylic acid in DMF performs equally well in dry and humid conditions for ammonia capture (2.2 mmol NH₃/g)¹³.

The “green” synthesis of MOFs, especially Al- and Zr-MOFs in water, is now well documented and has been recently reviewed²⁴ with a focus on requirements discussed by industrial research groups for MOF synthesis upscaling²⁵. Beyond the benefit presented by non-toxic solvents for the specific case of breathable filters, water-based synthesis would enable a substantial decrease in production costs²⁶. That said, it is now well known that different synthesis methods and work-up processes may yield different crystalline and porous structures, especially for UiO-66 type MOFs, for which the nature and concentration of defects are very process-sensitive^{27,28}. It has been shown that water adsorption properties, hydrophilicity and total water capacities depend on defect concentration in UiO-66^{29,30,31}. Hence, we can assume that NH₃ adsorption performance in humid conditions may also depend on the nature and concentration of defects resulting from different synthesis processes, which provides an additional reason for this investigation.

Here we present a benchmark study for the upscaled synthesis and shaping of UiO66-COOH that addresses key aspects for a potential industrialization, more specifically: (i) exclusive use of water for the synthesis, washing and shaping, (ii) use of non-explosive and non-corrosive starting chemicals, (iii) development of scalable shaping techniques and (iv) investigation of the mechanical and chemical stability of the shaped MOF. We show that the performances of the shaped UiO66-COOH are superior to those of commercial type K adsorbents for NH₃ air purification in relevant dynamic conditions covering a wide range of humidity levels. This paper can be regarded as a preliminary step toward a technical-economic study of UiO66-COOH as a type K air filter. The precise costs of large-scale production of a MOF and its shaping are beyond the scope of this study²⁶.

EXPERIMENTAL

Two types of commercial type K adsorbents were used here as benchmarks: (1) granules of activated carbon of 12–20 mesh¹⁸ commercialized by 3M and (2) Norit RZN1 extrudates of zinc salt-impregnated carbon. For breakthrough measurements, both materials were gently ground and sieved to obtain a fraction between 425 µm and 600 µm.

Small-scale synthesis of UiO66-COOH

A 10 mmol quantity of zirconium (IV) sulfate and 11 mmol of 1,2,4-benzenetricarboxylic acid were mixed together in 30 mL water. The synthesis was carried out under refluxing for 90 minutes. After that, the mixture was filtered, washed three times with distilled water on the filter

and dried in air at 120°C. After drying, 2.77 g of white powder was obtained, representing a yield of 87 wt.%.

Scaled-up synthesis of UiO66-COOH

A 12 L double-wall batch reactor was used. The reactant dispersion was mixed using an anchor-shaped mechanical stirrer at 100 rpm. An 8 L volume of deionized water and 1000 g (4.8 mol) of trimellitic acid from Sigma Aldrich were mixed together in a 12 L glass reactor. The initially white slurry became translucent above 70°C. The temperature inside the reactor reached 80°C after 2 h. At that moment, 736 g of zirconium sulfate tetrahydrate from Alfa-Aesar (2 mol) were added, and the mixture was kept under stirring for another 3 h while the temperature continued to increase. After 3 h, the temperature within the reactor reached 91°C. The heating was then switched off, and cooling was applied before the slurry was removed from the bottom of the reactor. The slurry was filtered on a Büchner-type setup, and then washed with 10 L of deionized water in three steps. The resulting white powder was then dried in an oven for 24 h at 120°C under air flow (1°C/min heating and cooling ramps). After drying, 647 g of white powder was obtained, representing a yield of 89 wt.%. The space-time yield was about 350 kg/day/m³.

For breakthrough measurements, 1.5 g of powder was pressed to pellets under a pressure of 97 bar using a die of 3 cm in diameter. A force of 5880 N was applied to the die and held for 1 minute. The resulting pellets were gently crushed and sieved in a particle size range between 425 µm and 600 µm.

Characterization

Powder X-ray diffraction (XRD) patterns of the solids were recorded on a Bruker (Siemens) D5005 diffractometer using Cu K α radiation. Diffractograms were collected between 4 and 80° (2θ) with steps of 0.02° and 1 s per step. N₂ isotherms at 77 K were measured by manometry using a BelMini device (BelJapan). Prior to measurement, the samples were activated under vacuum at 150°C overnight. The surface area and micropore volume were calculated using BET and t-plot methods, respectively. Particle size distribution analysis was conducted using a Microtrac S3500 laser granulometry apparatus. A very small amount of powder was dispersed in deionized water. In order to facilitate the desagglomeration, ultrasonic irradiation was applied for 30 s or 60 s. Thermogravimetric analysis (TGA) was carried out on a Mettler Toledo TGA-DSC1 apparatus using reconstituted air; in this case, UiO66-COOH powder was heated from 25°C to 800°C with a ramp of 5°C/min. Also, bulk densities of pellet, extrudates and beads of UiO66-COOH were measured. It corresponds to the ratio of the pellet mass or (n) extrudates or beads (n=10) to volume of each pellet, (n) extrudates or beads. Extrudates are cylinders with 3 mm length and 1.5 mm diameter. Beads are spheres of 3.76 mm. UiO66-COOH powder is compressed into a pellet of 3 cm diameter and 3 mm height.

Shaping by freeze granulation

Deionized water (74 vol.%) was mixed manually with a dispersant and binding agent (polyvinyl alcohol: 4 vol.% relative to the MOF). Subsequently, the MOF was added (22 vol.%). This mixture was then stirred manually again

prior to being transferred into a centrifugal vacuum mixer (Thinky ARV310), where it was exposed to a high stirring rate (2000 rpm, mixing time 2 minutes, with ZrO₂ mixing spheres) in order to disperse the particles and reduce agglomeration. Afterward, the suspension was separated from the mixing spheres by being cast through a 130 µm sieve and then poured into a syringe. Under controlled pressure the suspension was next deposited dropwise into liquid nitrogen. Upon contact with the liquid N₂, the drops of suspension instantaneously froze into spherical granules. These frozen beads were transferred to a freeze-dryer for sublimation of the solvent. As a result of this procedure, MOF beads were obtained; they averaged about 2.35 mm in diameter.

For micro-breakthrough measurements, the beads were gently ground and sieved to obtain a particle size range between 425 µm and 600 µm.

Shaping by extrusion

The extrusion paste was prepared using the kneading chamber of a Brabender Plastograph measuring kneader. A 60 g mass of MOF powder was placed inside the double-blade kneading chamber, and then water and the binder system were added under a constant rotational speed of 50 rpm. The mixing and plasticization process was performed for 30 min at room temperature. The prepared paste contained 72.5 vol.% UiO66-COOH, 22 vol.% water and 5.5 vol.% polysiloxane (silicon resin)-based binder. The extrusion was performed using laboratory piston extrusion equipment with a nozzle diameter of 1.5 mm. Lines of approximately 300 mm in length were extruded, dried at room temperature and then cut into small cylinders of about 1.5 mm length (hereafter referred to as extrudates).

For micro-breakthrough measurements, the cylinders were gently ground and sieved to obtain a granulometry between 425 µm and 600 µm.

Figure 1 shows the different shapes of UiO66-COOH and the commercial type K adsorbent.



Figure 1. Photographs of beads obtained by freeze granulation (left), extrudates (center) and commercial type K adsorbent from 3M (right).

Aging of UiO66-COOH

To investigate the impact of aging on ammonia adsorption performance, a compacted pellet of UiO66-COOH was aged under the same conditions as those reported by Hindocha et al.¹² at 80% RH for 7 days. Aged UiO66-COOH was tested under a flow of 1200 ppm NH₃ and 40% RH.

Attrition test of shaped UiO66-COOH

Attrition tests were conducted to assess the percentage amount of fine particles that the respective shaped materials can generate in the event of shaking or falling¹². A 0.2 g mass of material was introduced into a cylinder of 3 cm

internal diameter x 2.5 cm height containing an obstacle that the materials hit. This cylinder was made to turn on a classic tube roller (RSLAB-10) at a frequency of 60 rotations per minute (rpm) for 30 minutes. Afterward, the content was passed through a 425 µm sieve to recover fine particles. Attrition percentage is calculated as follows:

$$\text{Attrition} = \frac{\text{initial mass} - \text{recovered mass above } 425 \mu\text{m}}{\text{initial mass}} \times 100$$

Equation 1

Micro-breakthrough measurements

Assessment of NH₃ filtering was carried out by micro-breakthrough measurements similar to the methods reported elsewhere^{12,7}. The setup is presented in Figure 2. Humid conditions were generated by humidifying a controlled flow of diluted N₂ to obtain a stream of 100 mL/min with relative humidity of 40% or 70%. The concentration of NH₃ and water at the outlet were monitored online by an infrared spectrometer (Nicolet iS10 FT-IR) equipped with an insulated 2-meter gas cell (of 200 mL volume) from Thermo Fisher Scientific. A makeup flow of 440 mL/min was applied in order to renew the cell volume every 27 s, thus increasing the time resolution by a factor of approximately three. The frequency of acquisition was set to one analysis per 50 s.

The sieved powder (425-600 µm) was packed into a constant volume of 0.15 cm³ inside a 7-mm internal diameter fritted glass tube, to a height of 4 mm. The sieved fraction size, column dimension and flow rate are of the same order as those previously reported by Hindocha et al¹². The advantages of testing a sieved fraction are that (i) a relatively high flow rate can be used without a significant pressure drop, making it possible to discriminate between adsorbents with/without internal diffusion limitations¹ and (ii) it enables the comparison of adsorbents that were originally of different shapes and bulk densities since column packing and pressure drop should be the same.

Sorbents were first heated at 150°C for 30 minutes in flowing dry N₂. Breakthrough measurements were carried out at 22°C under 0% (dry), 40% and 70% RH in separate measurements starting with fresh samples. The challenge concentration was fixed at 1200 ppm NH₃ for 0% and 40% RH and at 600 ppm for 70% RH. For measurements under humid conditions, the sample was pre-equilibrated under humid stream flow at 40% or 70% RH. The water concentration at the outlet of the column was monitored until the adsorbent was saturated, permitting the water uptake at equilibrium to be quantified.

Micro-breakthrough graphs are plotted versus time in order to reflect the performance of the shaped materials for a given bed volume. The breakthrough time corresponds to the first time in minutes at which ammonia breaks through (concentration > 25 ppm) and is the relevant practical indicator for the performance of a shaped adsorbent because it defines the service life of the device. For comparison purposes with other studies, ammonia adsorption capacity is calculated by integrating under the breakthrough curve, using the trapeze method. The calculation of ammonia adsorption capacity W in mg is as follows:

$$W = (C_0 t_s - \sum_{t=0}^{t_s-1} \frac{C_n + C_{n-1}}{2} (t_n - t_{n-1})) \times \frac{F_t \times M \times 10^{-3}}{V_m}$$

Equation 2

The standard error is approximately 6%.

Plots of outlet ammonia concentration and corresponding uptake capacity expressed per unit of mass can be found in the SI.

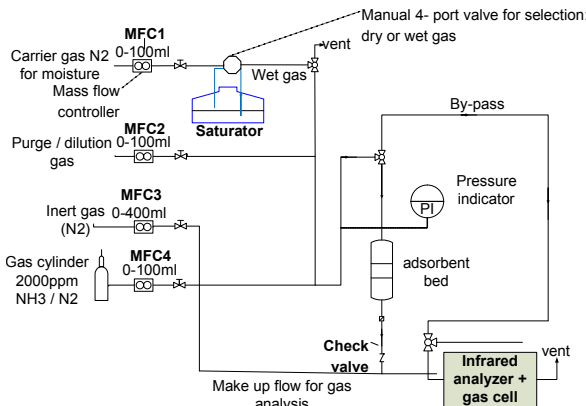


Figure 2. Diagram of the micro-breakthrough test rig.

RESULTS AND DISCUSSION

After the washing step, the powder obtained by large-scale synthesis was divided into four samples (Batch-1 to Batch-4) that were dried and characterized separately. Powder XRD, presented in Figure 3, shows highly crystalline samples that are very similar to those obtained from the small-batch synthesis. The patterns are also in excellent agreement with the theoretical pattern simulated from the reported crystal structure³². Finally, the TGA profile (Fig. S6) is also very similar to the data reported by Ragon et al³².

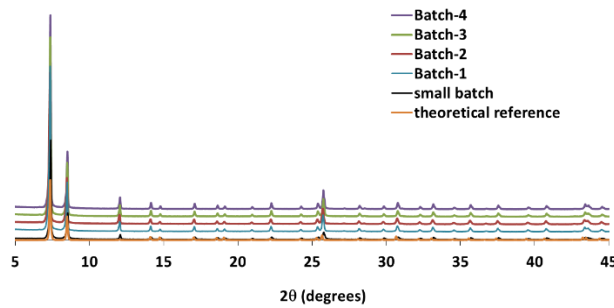


Figure 3. Powder X-ray diffractograms of the four samples from Batch-1 to -4 compared to the small-batch synthesis (black line) and to the theoretical reference (orange line).

Laser granulometry was applied to evaluate the size of the primary particles. The particle size distribution is shown in Figure 4. The as-activated powder presents particle sizes between 0.9 and 10 µm. After deagglomeration by ultrasonic irradiation, 90% of the particle size distribution is between 0.4 and 1 µm.

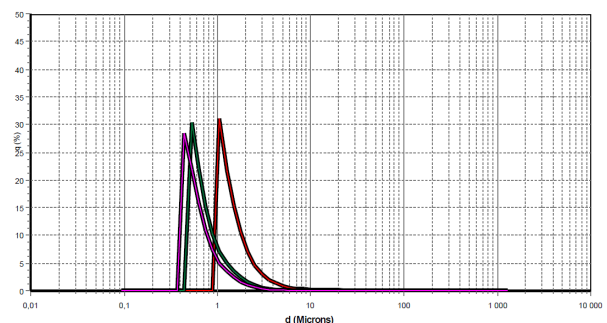


Figure 4. Particle size distribution of UiO-66-COOH (Batch-1) as-obtained (red), and after 30 s (green) and 60 s (pink) of ultrasonic irradiation.

Nitrogen adsorption isotherms are reported in Figure 5. High specific surface area ($710 \text{ m}^2/\text{g}$) and micropore volume ($0.28 \text{ cm}^3/\text{g}$) were obtained for an upscaled UiO66-COOH, in excellent agreement with Ragon et al³². While the compression is detrimental to the textural properties of the original UiO66-COOH powder, the specific surface areas of the extrudates and beads are about $418 \text{ m}^2/\text{g}$ and $359 \text{ m}^2/\text{g}$, respectively. We note, here, a decrease of about 50% in both the specific surface area and the micropore volume after freeze granulation and extrusion. This may be due to the addition of the plasticizer, which prevents N₂ from reaching the pore at 77 K compared to the original powder, and/or to anhydride formation from adjacent linkers upon heating, which has a direct impact on N₂ physisorption measurements³². We note a good correlation between water uptake at 40% relative humidity and the micropore volume measured by N₂ physisorption (Table 1).

The main difference between the shaped materials lies in their bulk density. While the compressed powder (tablet) presents a density of $0.62 \text{ cm}^3/\text{g}$, the extrudate is much denser at $1.04 \text{ cm}^3/\text{g}$, and the beads are much less dense at $0.12 \text{ cm}^3/\text{g}$. This contrast originates from the shaping techniques, which allow dissimilar crystallite packing and thus a specific macroporosity in the grain, the most porous form being the beads obtained by freeze granulation. As a direct consequence, NH₃ uptake values per unit of mass and volume strongly differ.

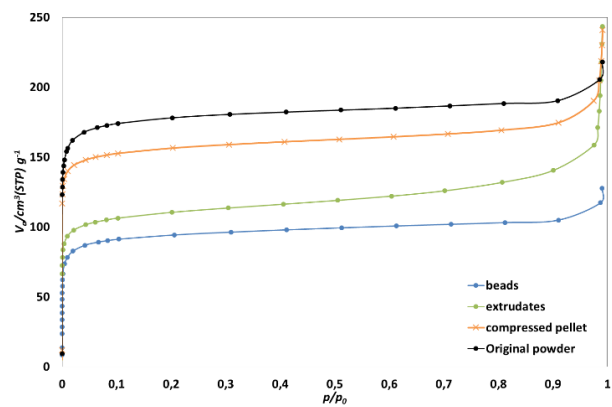


Figure 5. Nitrogen adsorption isotherms of the shaped UiO-66-COOH samples at 77 K.

Table 1. Textural properties of shaped UiO66-COOH

	Bulk density (g/cm ³)	Surface area § (m ² /g)	Micropore volume # (cm ³ /g)	Water uptake at RH=40% ε (cm ³ /g)
Original powder	n.a.	710	0.28	n.a.
Compressed Pellet	0.62	614	0.24	0.26
Extrudates	1.04	418	0.15	0.19
Beads	0.12	359	0.12	0.12

§ from BET analysis of N₂ physisorption at 77 K

from t-plot analysis of N₂ physisorption at 77 K

ε from micro-breakthrough measurements at 298 K

Figure 6, Figure 7 and Figure 8 represent ammonia breakthrough curves of shaped UiO66-COOH and commercial type K adsorbents under dry, wet conditions at 40 and 70% RH, respectively. We can observe that the breakthrough time and the profiles of the curves are relatively similar for the two benchmark adsorbents from 3M and Norit. We can also observe the same ranking of the adsorbents under dry and humid conditions. The UiO-COOH beads break first, followed by the AC reference materials, the compressed UiO-COOH and finally the extrudate. We notice that the shape of the breakthrough curves remains very similar regarding the rate at which the concentration increases when NH₃ breaks through, except for the beads, for which the breakthrough profile is much steeper. In this study, the grain sizes are identical because the samples were sieved from 425 µm to 600 µm, so we can rule out any differences in external diffusion processes. We suggest that the difference in the breakthrough slope could be caused by slow kinetics involving internal mass transfer limitations, as already reported for compressed pellets of UiO66-NH₂¹. We suppose that minor internal diffusion limitations could occur, i.e., inside the porosity of the grains, with the exception of the beads, which have a very high internal porosity.

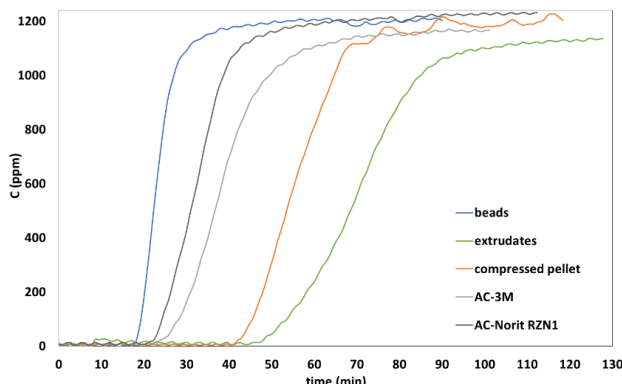


Figure 6. Comparison between ammonia breakthrough curves of commercial type K adsorbents as benchmark materials and shaped UiO66-COOH (1200 ppm NH₃, 0% RH).

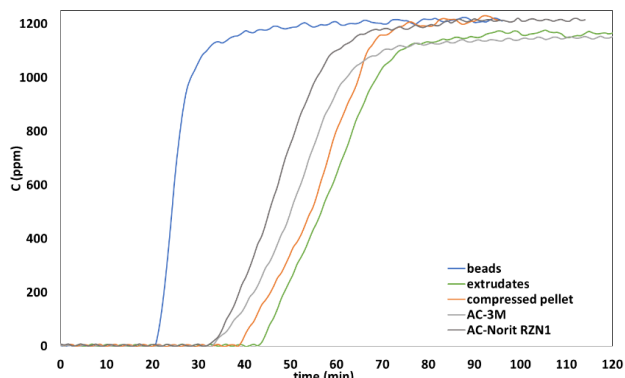


Figure 7. Comparison between ammonia breakthrough curves of commercial type K adsorbents as benchmark materials and shaped UiO66-COOH (1200 ppm NH₃, 40% RH).

Performance indicators of shaped MOFs and benchmark materials are summarized in Table 2. In practice, we could quantitatively rank the adsorbents by increasing breakthrough time because the measurements are carried out on the same bed volume. We found a relatively good correlation between the breakthrough time and the uptake capacity per unit volume (see SI). This linear correlation across the sample series arises from the similar wavefront profiles of the breakthrough curves. As a consequence, we prefer here to discuss the uptake values per unit volume rather than the breakthrough time values. The uptake values per unit mass can be calculated using the packed density values (see SI).

Under dry conditions (0% RH), UiO66-COOH compressed pellet and extrudates outperform by far the commercial adsorbents, with double breakthrough time and a noteworthy ammonia adsorption capacity (Figure 6). The uptake for the UiO66-COOH beads is much lower because of their very low density. However when compared on a mass basis, the beads rank at the same level as the 3M adsorbent.

At 40% relative humidity, the breakthrough time and ammonia uptakes are enhanced for the commercial adsorbents. A beneficial effect of humidity on NH₃ uptake in activated carbon-based adsorbents has already been reported elsewhere³³, while the mechanism of ammonia uptake in humid conditions has previously been found over a diverse set of adsorbents³⁴. In contrast to the activated carbons, the performances in humid conditions remain almost unchanged for the UiO-66-COOH compressed pellet and extrudates. At higher relative humidity (70%) and at 600 ppm of NH₃, the ammonia uptake for the UiO-66-COOH compressed pellet is 31 mg/cm³ versus 26 for the 3M adsorbent, which is also reflected by a longer breakthrough time, 81 min versus 75 min (c.f Figure 8).

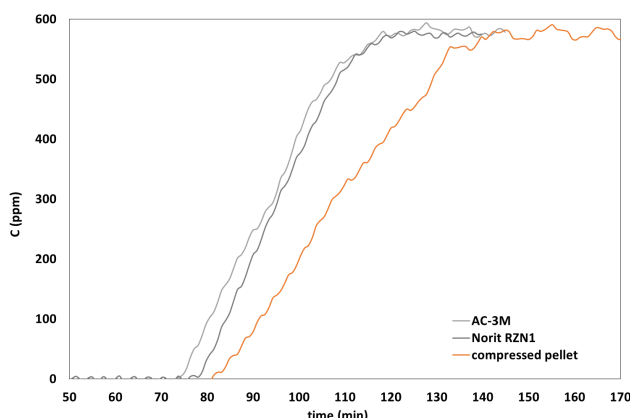


Figure 8. Comparison between ammonia breakthrough curves of commercial type K adsorbents as benchmark materials and compressed/sieved UiO66-COOH (600 ppm NH₃, 70% RH).

In all conditions tested, the UiO-66-COOH compressed pellet and extrudates outperform the commercial adsorbents in terms of capacity per unit volume and breakthrough time. The outstanding performances of UiO-66-COOH can be explained in part by the relatively high bulk density of the pellet and extrudates. In addition, even comparing the uptake by unit of mass, the UiO-66-COOH pellet and extrudates (55 and 53 mg/g, respectively) outperform the commercial Norit and 3M adsorbents (30 and 39 mg/g, respectively).

The ammonia uptake values in dry conditions obtained here are significantly higher than published data for UiO-66-COOH powders¹³. Here, we found uptakes of 55 mg/g as opposed to 38 mg/g¹³, which is significantly lower. The differences in uptakes may originate from different surface chemistry and/or concentration defects resulting from the synthesis process^{35,36,37}. While the upscaled synthesis is carried out here in water using Zr sulfate as precursor, the adsorbent in the literature¹³ was prepared in DMF starting with zirconium oxynitrate hydrate as precursor. We also note a major difference in the water uptake at 40% relative humidity, i.e., 0.26 cm³/g in this study compared to 0.04 cm³/g for Joshi et al.¹³, while both solids exhibit almost the same micropore volumes of 0.24 cm³/g and 0.28 cm³/g, respectively. This simultaneous difference in water uptake and near-sameness of micropore volume supports the assumption that the synthesis in water may generate a higher concentration of surface hydroxyl groups, which are favorable for water and ammonia adsorption^{29,30,31}.

Regenerability of UiO66-COOH was tested by reactivating the material at 150°C with a ramp of 10°C/min, under 100 ml/min N₂, then conducting a second cycle of am-

nia adsorption. Corresponding breakthrough curves for recycled compressed pellet at dry and humid conditions are reported in the SI (c.f. Figure S4 and S5). These curves reveal that UiO66-COOH is regenerable at 70% and 77% in term of ammonia adsorption capacity at dry and humid conditions, respectively. We conclude that UiO66-COOH could be regenerable at the level of 100% by increasing the regeneration temperature. (on peut nous dire que le MOF risque de se détruire en élévant la température, mais bon un Zr-MOF tiens)

Finally, the robustness of the shaped UiO-66-COOH has been verified. The stability upon shaking was measured by an attrition test similar to that reported by Hindocha¹² and that corresponds to a downscaled device from the D4058-96 (2011) ASTM norm. After shaking the beads, the extrudates or the pellets in a cylinder for 30 minutes at 60 rpm, the weight loss due to attrition is below 2 wt.% which is an excellent value, while for the Norit extrudates it is below 1 wt.%.

Pellets of UiO-66-COOH were aged for 7 days at 80% RH as mentioned in Hindocha et al.¹². Breakthrough curves of initial and aged extrudates are compared in Figure 9 and corresponding performance indicators are included in Table 1. We observe that the aged UiO-66-COOH breaks through 8 minutes earlier with very similar uptake (34 mg/cm³ compared to 33 mg/cm³). At this stage we cannot provide insights explaining the modification of the curve, which would merit a detailed study beyond the scope of this paper. Nevertheless, we want to point out that even after aging, the UiO-66-COOH pellet always outperforms the two commercial benchmark adsorbents.

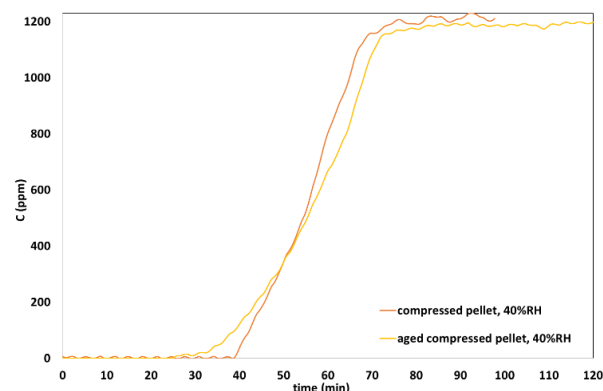


Figure 9. Comparison between ammonia breakthrough curves of fresh and aged compressed pellets of UiO66-COOH (1200 ppm NH₃, 40% RH).

Table 2. Ammonia adsorption capacities and breakthrough times under dry and wet conditions.

	Packed bed density (425–600 µm) (g/cm ³)	Attrition (%)	Ammonia adsorption amount (mg/cm ³)			Breakthrough time (min)		
			1200 ppm		600 ppm	1200 ppm		600 ppm
			0% RH	40% RH	70% RH	0% RH	40% RH	70% RH
Compressed pellet	0.6	1.7	33	33	31	41	40	81
Aged compressed pellet	0.6	-		34	-		32	-
Extrudates	0.7	1.4	40	34	n.d.	48	43	n.d.
Beads	0.4	0	14	16	n.d.	18	20	n.d.
AC-3M	0.5	0	23	29	26	24	32	75
AC-Norit RZN1	0.7	0.2	20	29	27	21	32	78

CONCLUSION

Metal-Organic Frameworks attract considerable interest in general and particularly for air purification. The industrialization of an adsorbent is not a straightforward task, however, because the upscaled synthesis and shaping process may alter the final performance of the original powder. Herein we have presented a high-yield synthesis of UiO66-COOH by precipitation of a non-corrosive salt. In addition, the fast reaction and the easy recovery and washing should make this process feasible at the industrial scale. The particularly elevated ammonia uptake possibly arises from a higher surface hydrophilicity resulting from a higher hydroxyl surface concentration than that found with the original synthesis in DMF.

The high grain density achieved by extrusion and compression in pellets makes UiO66-COOH a very efficient adsorbent for NH₃ air purification that outperforms commercial benchmarks, especially in dry conditions, in which the ammonia uptake and service life of the commercial adsorbent are compromised. Mechanical stability and aging upon exposure to humidity were verified.

Full-scale testing in a separation device is beyond the scope of this paper and will be published elsewhere.

ASSOCIATED CONTENT

Supporting Information. Ammonia breakthrough curves on a mass-weighted basis and ammonia adsorption capacities, breakthrough times on a mass-weighted basis under dry and wet conditions, correlation graph between breakthrough time and uptake capacity per unit volume and TGA profile of UiO66-COOH. This material is available free of charge via the Internet at <http://pubs.acs.org>.

AUTHOR INFORMATION

Corresponding Author

* david.farrusseng@ircelyon.univ-lyon1.fr

Author Contributions

The manuscript was written through contributions of all authors. All authors have given approval to the final version of the manuscript.

Funding Sources

This work has been carried out within the ProDIA project, which has received funding from the European Union's Horizon 2020 research and innovation program under grant agreement No. 685727.

ABBREVIATIONS

C ₀	Ammonia challenge concentration (ppm)
C	Ammonia concentration at time (t) (ppm)
F _t	Total flow (mL/min)
M	Ammonia molar mass (g/mol)
t _s	time until saturation
V _m	Molar volume (m ³ /mol)

REFERENCES

- (1) Peterson, G. W.; DeCoste, J. B.; Fatollahi-Fard, F.; Britt, D. K. Engineering UiO-66-NH₂ for Toxic Gas Removal. *Ind. Eng. Chem. Res.* **2014**, *53* (2), 701.
- (2) Peterson, G. W.; Wagner, G. W.; Balboa, A.; Mahle, J.; Sewell, T.; Karwacki, C. J. Ammonia Vapor Removal by Cu₃(BTC)₂ and Its Characterization by MAS NMR. *J. Phys. Chem. C* **2009**, *113* (31), 13906.
- (3) Moghadam, P. Z.; Fairen-Jimenez, D.; Snurr, R. Efficient Identification of Hydrophobic MOFs: Application in the Capture of Toxic Industrial Chemicals. *J. Mater. Chem. A* **2016**, *4* (2), 529.
- (4) Gonçalves, M.; Sánchez-García, L.; Oliveira Jardim, E. de; Silvestre-Albergo, J.; Rodríguez-Reinoso, F. Ammonia Removal Using Activated Carbons: Effect of the Surface Chemistry in Dry and Moist Conditions. *Environ. Sci. Technol.* **2011**, *45* (24), 10605.
- (5) Matthew A. Browea, Amedeo Napolitano, Jared B. De Coste, G. W. P. Filtration of Chlorine and Hydrogen Chloride Gas by Engineered UiO-66-NH₂ Metal-Organic Framework. *J. Hazard. Mater.* **2017**, *332*, 162.
- (6) Nijem, N.; Fürschich, K.; Bluhm, H.; Leone, S. R.; Gilles, M. K. Ammonia Adsorption and Co-Adsorption with Water in HKUST-1: Spectroscopic Evidence for Cooperative Interactions. *J. Phys. Chem. C* **2015**, *119* (44), 24781.
- (7) Jasuja, H.; Peterson, G. W.; Decoste, J. B.; Browne, M. A.; Walton, K. S. Evaluation of MOFs for Air Purification and Air Quality Control Applications: Ammonia Removal from Air. *Chem. Eng. Sci.* **2015**, *124*, 118.

- (8) Kim, K. C.; Yu, D.; Snurr, R. Q. Computational Screening of Functional Groups for Ammonia Capture in Metal–Organic Frameworks. *Langmuir* **2013**, *29* (5), 1446.
- (9) Grant Glover, T.; Peterson, G. W.; Schindler, B. J.; Britt, D.; Yaghi, O. MOF-74 Building Unit Has a Direct Impact on Toxic Gas Adsorption. *Chem. Eng. Sci.* **2011**, *66* (2), 163.
- (10) Barea, E.; Montoro, C.; Navarro, J. A. R. Toxic Gas Removal–Metal–Organic Frameworks for the Capture and Degradation of Toxic Gases and Vapours. *Chem. Soc. Rev.* **2014**, *43* (16), 5419.
- (11) DeCoste, J. B.; Peterson, G. W. Metal–Organic Frameworks for Air Purification of Toxic Chemicals. *Chem. Rev.* **2014**, *114* (11), 5695.
- (12) Hindocha, S.; Poulston, S. Study of the Scale-Up, Formulation, Ageing and Ammonia Adsorption Capacity of MIL-100(Fe), Cu-BTC and CPO-27(Ni) for Use in Respiratory Protection Filters. *Faraday Discuss.* **2017**, *201* (0), 113.
- (13) Joshi, J. N.; Garcia-Gutierrez, E. Y.; Moran, C. M.; Deneff, J. I.; Walton, K. S. Engineering Copper Carboxylate Functionalities on Water Stable Metal–Organic Frameworks for Enhancement of Ammonia Removal Capacities. *J. Phys. Chem. C* **2017**, *121* (6), 3310.
- (14) Mounfield, W. P.; Taborga Claure, M.; Agrawal, P. K.; Jones, C. W.; Walton, K. S. Synergistic Effect of Mixed Oxide on the Adsorption of Ammonia with Metal–Organic Frameworks. *Ind. Eng. Chem. Res.* **2016**, *55* (22), 6492.
- (15) Gregory W. Peterson, Jared B. DeCoste, T. Grant Glover, Yougui Huang, H. J.; Walton, K. S. Effects of Pelletization Pressure on the Physical and Chemical Properties of the Metal–organic Frameworks Cu₃(BTC)₂ and UiO-66. *Microporous Mesoporous Mater.* **2013**, *179*, 48.
- (16) Hazardous Substance Fact Sheet for Dimethylformamide.
- (17) Hurtt, M. E.; Placke, M. E.; Killinger, J. M.; Singer, A. W.; Kennedy, G. L. 13-Week Inhalation Toxicity Study of Dimethylformamide (DMF) in Cynomolgus Monkeys. *Fundam. Appl. Toxicol.* **1992**, *18* (4), 596.
- (18) Andrew R. Fox, J. M. L. Air Filter with Sorbent Particles. US Patent 9539532 B2, 2011.
- (19) Beckner, M.; Dailly, A. A Pilot Study of Activated Carbon and Metal–organic Frameworks for Methane Storage. *Appl. Energy* **2016**, *162*, 506.
- (20) Dhainaut, J.; Avci-Camur, C.; Troyano, J.; Legrand, A.; Canivet, J.; Imaz, I.; Maspoch, D.; Reinsch, H.; Farrusseng, D. Systematic Study of the Impact of MOF Densification into Tablets on Textural and Mechanical Properties. *CrystEngComm* **2017**, *19* (29), 4211.
- (21) DeCoste, J. B.; Peterson, G. W.; Jasuja, H.; Glover, T. G.; Huang, Y.; Walton, K. S. Stability and Degradation Mechanisms of Metal–Organic Frameworks Containing the Zr₆O₄(OH)₄ Secondary Building Unit. *J. Mater. Chem. A* **2013**, *1* (18), 5642.
- (22) Kandiah, M.; Nilsen, M. H.; Usseglio, S.; Jakobsen, S.; Olsbye, U.; Tilset, M.; Larabi, C.; Quadrelli, E. A.; Bonino, F.; Lillerud, K. P. Synthesis and Stability of Tagged UiO-66 Zr-MOFs. *Chem. Mater.* **2010**, *22* (24), 6632.
- (23) Wang, B.; Ly, X.-L.; Feng, D.; Xie, L.-H.; Zhang, J.; Li, M.; Xie, Y.; Li, J.-R.; Zhou, H.-C. Highly Stable Zr(IV)-Based Metal–Organic Frameworks for the Detection and Removal of Antibiotics and Organic Explosives in Water.
- (24) Reinsch, H. “Green” Synthesis of Metal–Organic Frameworks. *Eur. J. Inorg. Chem.* **2016**, *2016* (27), 4290.
- (25) Gaab, M.; Trukhan, N.; Maurer, S.; Gummaraju, R.; Müller, U. The Progression of AI-Based Metal–Organic Frameworks – From Academic Research to Industrial Production and Applications. *Microporous Mesoporous Mater.* **2012**, *157*, 131.
- (26) DeSantis, D.; Mason, J. A.; James, B. D.; Houchins, C.; Long, J. R.; Veenstra, M. Techno-Economic Analysis of Metal–Organic Frameworks for Hydrogen and Natural Gas Storage.
- (27) Shearer, G. C.; Chavan, S.; Ethiraj, J.; Vitillo, J. G.; Svelle, S.; Olsbye, U.; Lamberti, C.; Bordiga, S.; Lillerud, K. P. Tuned to Perfection: Ironing Out the Defects in Metal–Organic Framework UiO-66. *Chem. Mater.* **2014**, *26* (14), 4068.
- (28) Shearer, G. C.; Chavan, S.; Bordiga, S.; Svelle, S.; Olsbye, U.; Lillerud, K. P. Defect Engineering: Tuning the Porosity and Composition of the Metal–Organic Framework UiO-66 via Modulated Synthesis.
- (29) Liang, W.; Coglan, C. J.; Ragon, F.; Rubio-Martinez, M.; D’Alessandro, D. M.; Babarao, R. Defect Engineering of UiO-66 for CO₂ and H₂O Uptake - a Combined Experimental and Simulation Study. *Dalt. Trans.* **2016**, *45* (11), 4496.
- (30) Taddei, M. When Defects Turn into Virtues: The Curious Case of Zirconium-Based Metal–Organic Frameworks. *Coord. Chem. Rev.* **2017**, *343* (Supplement C), 1.
- (31) Ghosh, P.; Colon, Y. J.; Snurr, R. Q. Water Adsorption in UiO-66: The Importance of Defects. *Chem. Commun.* **2014**, *50* (77), 11329.
- (32) Ragon, F.; Campo, B.; Yang, Q.; Martineau, C.; Wiersum, A. D.; Lago, A.; Guillerm, V.; Hemsley, C.; Eubank, J. F.; Vishnuvarthan, M.; Taulelle, F.; Horcajada, P.; Vimont, A.; Llewellyn, P.L.; Daturi, M.; Devautour-Vinot, S.; Maurin, G.; Serre, C.; Devic, T.; Clet, G. Acid-Functionalized UiO-66(Zr) MOFs and Their Evolution after Intra-Framework Cross-Linking: Structural Features and Sorption Properties. *J. Mater. Chem. A* **2015**, *3* (7), 3294.
- (33) Lodewyckx, P. Chapter 10 Adsorption of Chemical Warfare Agents. *interface Sci. Technol.* **2006**, *7*, 475.
- (34) Khabzina, Y.; Farrusseng, D. Unravelling Ammonia Adsorption Mechanisms of Microporous Adsorbents in Humid Conditions. *Microporous Mesoporous Mater.* **2018**, *265* (15), 143.
- (35) Vandichel, M.; Hajek, J.; Vermoortele, F.; Waroquier, M.; De Vos, D. E.; Van Speybroeck, V. Active Site Engineering in UiO-66 Type Metal–Organic Frameworks by Intentional Creation of Defects: A Theoretical Rationalization. *CrystEngComm* **2015**, *17* (2), 395.
- (36) Vandichel, M.; Hajek, J.; Ghysels, A.; De Vos, A.; Waroquier, M.; Van Speybroeck, V. Water Coordination and Dehydration Processes in Defective UiO-66 Type Metal Organic Frameworks. *CrystEngComm* **2016**, *18* (37), 7056.
- (37) Valenzano, L.; Civalleri, B.; Chavan, S.; Bordiga, S.; Nilsen, M. H.; Jakobsen, S.; Lillerud, K. P.; Lamberti, C. Disclosing the Complex Structure of UiO-66 Metal Organic Framework: A Synergic Combination of Experiment and Theory. *Chem. Mater.* **2011**, *23* (7), 1700.

